2018

Chemoselective Hydrogenation with Supported Organoplatinum(IV) Catalyst on Zn(II)-Modified Silica

Jeffrey Camacho-Bunquin
Argonne National Laboratory

Magali Ferrandon
Argonne National Laboratory

Hyuntae Sohn
Argonne National Laboratory

Dali Yang
Argonne National Laboratory

Cong Liu
Argonne National Laboratory

See next page for additional authors

Chemoselective Hydrogenation with Supported Organoplatinum(IV) Catalyst on Zn(II)-Modified Silica

Abstract
Well-defined organoplatinum(IV) sites were grafted on a Zn(II)-modified SiO2 support via surface organometallic chemistry in toluene at room temperature. Solid-state spectroscopies including XAS, DRIFTS, DRUV–vis, and solid-state (SS) NMR enhanced by dynamic nuclear polarization (DNP), as well as TPR-H2 and TEM techniques revealed highly dispersed (methylcyclopentadienyl)methylplatinum(IV) sites on the surface ((MeCp)PtMe/Zn/SiO2, **1**). In addition, computational modeling suggests that the surface reaction of (MeCp)PtMe3 with Zn(II)-modified SiO2 support is thermodynamically favorable (ΔG = −12.4 kcal/mol), likely due to the increased acidity of the hydroxyl group, as indicated by NH3-TPD and DNP-enhanced 17O{1H} SSNMR. *In situ* DRIFTS and XAS hydrogenation experiments reveal the probable formation of a surface Pt(IV)-H upon hydrogenolysis of Pt-Me groups. The heterogenized organoplatinum(IV)-hydride sites catalyze the selective partial hydrogenation of 1,3-butadiene to butenes (up to 95%) and the reduction of nitrobenzene derivatives to anilines (up to 99%) with excellent tolerance of reduction-sensitive functional groups (olefin, carbonyl, nitrile, halogens) under mild reaction conditions.

Disciplines
Chemistry | Inorganic Chemistry | Materials Chemistry

Authors
Jeffrey Camacho-Bunquin, Magali Ferrandon, Hyuntae Sohn, Dali Yang, Cong Liu, Patricia Anne Ignacio-de Leon, Frederic A. Perras, Marek Pruski, Peter C. Stair, and Massimiliano Delferro

Chemoselective Hydrogenation with Supported Organoplatinum(IV) Catalyst on Zn(II)-Modified Silica

Jeffrey Camacho-Bunquin,[a]* Magali Ferrandon,[a] Hyuntae Sohn,[a] Dali Yang,[a] Cong Liu,[a] Patricia Anne Ignacio-de Leon,[b] Frédéric A. Perras,[c] Marek Pruski,[c,d] Peter C. Stair [a,e]* and Massimiliano Delferro[a]*

[a]Chemical Sciences and Engineering Division, Argonne National Laboratory, 9700 S Cass Avenue, Lemont, Illinois 60439, United States

[b]Energy Sciences Division, Argonne National Laboratory, 9700 S Cass Avenue, Lemont, Illinois 60439, United States

[c]Ames Laboratory, U.S. Department of Energy, Ames, Iowa, 50010, United States

[d]Department of Chemistry, Iowa State University, 2416 Pammel Drive, Ames, Iowa, 50011, United States

[e]Department of Chemistry, Northwestern University, 2145 Sheridan Road, Evanston, Illinois 60208, United States

ABSTRACT: Well-defined organoplatinum(IV) sites were grafted on a Zn(II)-modified SiO_2 support via surface organometallic chemistry in toluene at room temperature. Solid-state spectroscopies including XAS, DRIFTS, DRUV-Vis, and solid-state (SS) NMR enhanced by dynamic nuclear polarization (DNP), as well as TPR-H_2 and TEM techniques revealed highly dispersed (methylcyclopentadienyl)methylplatinum(IV) sites on the surface ((MeCp)PtMe/Zn/SiO_2, **1**). In addition, computational modelling suggests that the surface reaction of (MeCp)$PtMe_3$ with Zn(II)-modified SiO_2 support is thermodynamically favorable (ΔG = -12.4 kcal/mol), likely due to the increased acidity of the hydroxyl group, as indicated by NH_3-TPD and DNP-enhanced $^{17}O\{^1H\}$ SSNMR. *In situ* DRIFTS and XAS hydrogenation experiments reveal the likely formation of a surface Pt(IV)-H upon hydrogenolysis of Pt-Me groups. The heterogenized organoplatinum(IV)-hydride sites catalyze the selective partial hydrogenation of 1,3-butadiene to butenes (up to 95%) and the reduction of nitrobenzene derivatives to anilines (up to 99%) with excellent tolerance of reduction-sensitive functional groups (olefin, carbonyl, nitrile, halogens) under mild reaction conditions.

Introduction

Chemoselective catalytic hydrogenation plays an important role for the production of fine chemicals.[1] In particular, the chemoselective hydrogenation of functionalized nitro-aromatics to aromatic amines is an industrially important transformation, principally in the agrochemical, pigment and pharmaceutical industries.[2] Catalysts that preferentially reduce nitro groups and are tolerant of other hydrogenation-sensitive functionalities, such as C=C and C=O groups, are desired for this chemistry. Current industrial strategies for the reduction of nitro-aromatics employ stoichiometric quantities of reducing agents (e.g., sodium hydrosulfide, iron, tin or zinc in ammonium hydroxide),[3] and noble metal hydrogenation catalysts (e.g., Pb–Pt/$CaCO_3$, Pt/C)[4] in the presence of transition metal additives (e.g., Fe and V salts).[4b, 5] Additive-free and recyclable nitro-aromatic hydrogenation catalysts recently became available after the development of supported Au nanoparticles on oxides such as TiO_2 and Fe_2O_3,[4b] Au alloys with hydrogenation-active metals such as Pd or Pt,[6] transition metal nanoparticles such as Pt, Ru or Ni,[6-7] and single-atom noble metal catalysts (e.g., Pt/FeO_x).[4] With the ever-increasing cost of noble metals and their fairly low natural abundance, additive-free, atom-efficient and recyclable catalyst strategies will ensure the long-term sustainability of this industrial catalytic process.[8]

Corma and coworkers[9] recently demonstrated that downsizing of supported Pt sites from nanoparticles to highly dispersed clusters or single-atom catalytic sites in a Pt/FeO_x system resulted in catalytic materials with unprecedented reactivity and enhanced selectivity for hydrogenation of poly-functionalized nitro-aromatics to the aromatic amines. The Pt/FeO_x systems were synthesized via co-precipitation of noble metals with bulk, low-surface-area metal oxides (FeO_x),[4b, 10] resulting in some of the Pt sites entrapped in the bulk of the material. Additionally, the low surface area of these systems can limit the number of accessible catalytic surface sites. Conceivably, high-surface-area oxides, such as silica, comprise a promising class of supports for isolated noble metal catalysts. The low acidity and weak interaction of SiO_2 with noble metals, however, render such a support less effective in stabilizing noble metal active sites.

Surface organometallic chemistry (SOMC)[11,12,13,14,15] represents an alternative synthetic strategy for the controlled deposition of highly-dispersed, single-site catalysts on traditional high-surface-area supports. Over the past few decades, SOMC has been employed in the synthesis of oxide-supported metallic catalysts for chemoselective hydrogenation of a range of unsaturated organics such as alkenes, carbonyls and α,β-unsaturated carbonyls.[14g, 16] The reactivity of surface organometallic catalytic sites can be tuned/influenced by ancillary ligands

and/or metal-hydrocarbyl moieties, with the latter purposefully incorporated as a convenient entry into the target catalytic cycle via activation under reducing conditions.[17]

Here we report the design, synthesis and characterization of a supported organoplatinum catalyst for selective hydrogenation of organic substrates, where isolated organoplatinum(IV) sites were deposited on a Zn(II)-modified SiO_2 surface via SOMC. The synthetic approach involves the installation of a submonolayer of Zn^{2+} anchoring sites on SiO_2 to stabilize highly dispersed organoplatinum(IV) fragments. In this system, the Pt^{4+} sites are bound to the surface, predominantly in a bipodal fashion and stabilized by the methylcyclopentadienyl ligand and one methyl group ((MeCp)PtMe/Zn/SiO_2, **1**). The hydrogenolysis of **1** leads to the likely formation of a catalytically active organoplatinum(IV) hydride species, ((MeCp)PtH/Zn/SiO_2, **2**), as observed by *in situ* infrared spectroscopy. The resulting $Pt^{4+}/Zn^{2+}/SiO_2$ catalyst exhibits hydrogenation activity well differentiated from its PtZn/SiO_2 nanoparticle counterparts;[18] catalyst **2** semi-hydrogenates 1,3-butadiene to mixtures of butenes, and chemoselectively hydrodeoxygenates a range of functionalized nitro-aromatics to the corresponding anilines, under mild conditions. Investigation of the effects of catalyst activation conditions revealed that hydrogenolysis of the (MeCp)-Pt linkage is detrimental to the hydrogenation selectivity, confirming that supported organoplatinum active species are responsible for the chemoselective catalysis.

Experimental Section

Materials and Methods. All manipulations of air-sensitive materials were performed with rigorous exclusion of O_2 and moisture in oven-dried Schlenk-type glassware on a dual manifold Schlenk line or in a N_2-filled MBraun glovebox with a high-capacity recirculator (<1 ppm O_2), unless noted otherwise. Silica (Davisil 646, 40−50 mesh, 300 m^2/g), methylcyclopentadienyltrimethylplatinum(IV) and diethyl zinc were used as received (Sigma-Aldrich). All gases (1% 1,3-butadiene/He, 10% H_2/N_2, 100% H_2, and N_2) were purchased from Airgas as UHP grade and had oxygen and moisture traps. Solid substrates, 2-nitrobenzaldehyde, 4-nitrobenzaldehyde, 4-nitrobenzophenone, methyl 4-nitrobenzoate, 4-nitrobenzonitrile, and 2-chloronitrobenzene, were purchased from Sigma-Aldrich and dried in a flask with a Teflon stopcock under vacuum at ambient temperature for 16 h before use. Liquid substrates such as 3-nitrostyrene, 4-nitrostyrene, and nitrobenzene, were purchased from Sigma-Aldrich and sparged with N_2 for an hour prior to use. Dodecane (Sigma-Aldrich) was sparged with nitrogen and dried over activated alumina.

Synthesis of (MeCp)PtMe/Zn/SiO_2 (1) and (MeCp)PtH/Zn/SiO_2 (2) Materials. Zn^{2+} was installed on SiO_2 via atomic layer deposition (ALD) using an ARRADIANCE Integrated ALD-Catalysis tool (model ARR-100000 GEMSTAR-CAT Dual System)[19] according the literature procedure[20] (10% w/w; 75% of a theoretical monolayer; see also Supporting Information). A 40 mL scintillation vial was charged with a slurry of 2.0 g Zn/SiO_2 in 10 mL toluene. A 20 mL toluene solution of [(MeCp)$PtMe_3$] (390 mg, 1.22 mmol Pt) was added drop-wise to the stirring slurry of Zn/SiO_2 over 30 minutes. The reaction mixture was stirred for 24 h, the stirring stopped, and the resulting solids filtered. The resulting (MeCp)PtMe/Zn/SiO (**1**) solid was then washed with two 10 mL portions of toluene and was dried under vacuum. The metal loading of **1** product was determined by ICP-OES: Pt = 0.2 % (w/w), Zn = 10%. For the catalysis experiments described below, pre-catalyst **1** is activated with H_2 over a range of temperatures. Activation at a temperature of 135 °C results in an active hydrogenation catalyst **2**.

Synthesis of PtZn/SiO_2 (nanoparticles) Catalyst (3). The as-prepared (MeCp)PtMe/Zn/SiO (**1**) was loaded in a tube furnace, dried at 150 °C for 2 h, and then calcined with a flow of air at 550 °C for 4 h.

Physical and Analytical Measurements. Elemental analysis (Pt, Zn) was conducted by Galbraith Laboratories, Inc. (Knoxville, TN). Temperature-programmed reduction (TPR-H_2) and ammonia-temperature programmed desorption (NH_3-TPD) were performed on an Altamira catalyst characterization instrument (model: AMI-200-MR). For TPR-H_2, 40 mg of **1** was first measured and transferred into a quartz tube forming a catalyst bed. The quartz reactor was then centered inside a lab-scale furnace. A thermocouple was attached at the inlet of the reactor having a close contact with the sample to measure the actual temperature of the catalyst bed. The outlet of the reactor was connected to a thermal conductivity detector (TCD) followed by a Dycor Benchtop Mass Spectrometer (AMETEK Process Instrument). A gas mixture of 3% H_2/Ar was introduced to the reactor at 30 mL/min while the reactor temperature was increased from RT to 600 °C with a ramp rate of 10 °C/min. The TCD and mass spectrometer signals were collected continuously (m/z = 2 to 50) during the reaction. Similarly, the NH_3-TPD experiment was conducted using 1% NH_3/Ar gas. The sample was first treated with pure Ar at 200 °C for 60 min. The temperature was then decreased to 100 °C and 1% NH_3/Ar was introduced to the reactor for 60 min to adsorb NH_3 on the catalyst surface. The NH_3 desorption was performed by increasing the reactor temperature from 100 °C to 650 °C at a ramp rate of 10 °C/min and held at 650 °C for 60 min. The exhaust stream from the reactor was analyzed by both TCD and mass spectrometer (m/z = 16, 17) detectors.

Diffuse reflectance infrared Fourier transform spectroscopy (DRIFTS) was acquired using a Thermo Scientific™ Nicolet iS50 FT-IR spectrometer equipped with an iS50 Automated Beam splitter exchanger (ABX). Pre-catalyst **1** was finely ground and placed on a sample holder inside a high temperature reaction chamber (Praying Mantis™). The DRIFTS spectra of pre-catalyst **1** were collected at RT under He and at 100 °C and 150 °C under reducing conditions (H_2) using 30 mL/min of 3% H_2/He. A spectrum of SiO_2 was obtained separately and was used as a background for all three temperatures. The detection of Pt-H was carried out using the same reactor. For this experiment, pre-catalyst **1** with higher Pt loading (1% w/w) was employed in order to match the detection level of the DRIFTS instrument. The tested sample was not exposed to air after Pt grafting on Zn/SiO_2 to reduce the undesirable interference from water. First, a background spectrum was collected after purging pre-catalyst **1** at RT for 10 min with He at 30 mL/min. The sample was then exposed to 30 mL/min of pure H_2 at RT for 30 min. After a spectrum was collected, which served as the background for subsequent measurements, the reactor temperature was increased to 50 °C, 100 °C, 135 °C and 150 °C. At each temperature, the sample was treated with pure H_2 for 30 min (30 mL/min) and a spectrum was obtained. Identical experimental procedures were followed to observe Pt-D employing a pure D_2 gas at 30 mL/min. Lastly, the spectrum of CO adsorbed on **1** was recorded before and after H_2 reduction

first at 100 °C and then at 200 °C. The experimental procedure was as follows: 1) the reactor cell was flushed with He at 30 mL/min while the temperature of the reactor cell was increased from RT to 40 °C. 2) A background spectrum of **1** was collected at 40 °C after flushing for 10 min in He. 3) The sample was then treated with 10% CO/He at 30 mL/min for 1 h and a spectrum was collected. 4) Another spectrum was recorded after flushing with He for 10 min. For H_2 treated samples, 30 mL/min of 3% H_2/He gas was introduced to the reactor cell at 100 °C or 200 °C for 1 h and then cooled down to RT in He prior to step 1).

The diffuse reflectance ultraviolet-visible (DRUV-Vis) spectra were obtained on a Shimadzu UV-3600 Plus spectrophotometer using a photomultiplier tube (PMT) detector. The samples were first finely ground and placed on a cup holder where the beam was aligned at the center. The measurement was done using a medium scan speed, 1 nm sampling interval and a slit width of 3 nm. Two reference spectra of polytetrafluoroethylene (PTFE) and SiO_2 were collected from 200 to 700 nm and used as backgrounds (R_{ref}). The obtained sample spectra were transformed to Kubelka-Munk (K-M) and Tauc functions using the equation $F(R_\infty)=(1-R_1)^2/2\times R_1$ where R_∞ denotes K-M function and $R_1=R_{sample}/R_{ref}$. All the samples were diluted using SiO_2 to reduce the K-M intensity below 1.5. The dilution was carried out in order to eliminate nonlinearity while collecting the spectra.

A JEOL JEM-2100F transmission electron microscope (TEM) was used for all bright field (BF) imaging at 200 kV. Samples were prepared by dispersing solids in ethanol via sonication for 30 s. Colloidal suspensions were drop cast onto lacey C on Cu grids (300 mesh) from Electron Microscopy Sciences.

The crystalline phase compositions of spent catalyst **2** (after 24 h reaction at 75 °C in 0.25 M nitrobenzene with 200 psi H_2) were determined by powder X-ray diffraction (PXRD) using a Bruker Diffractometer D8 Advance operating with the following parameters: Cu Kα radiation of 40 mA, 40 kV, K_λ = 0.15418 nm, 2θ scanning range of 10-70°, a scan step size of 0.0018º and a time of 1s per step. The sample was ground and placed on a zero background silicon holder (MTI Corp.) for analysis.

Computational Details. All the calculations were carried out using B3LYP functional[21] with a CEP-31G basis set[22] as available for the E.01 version of the Gaussian09 program.[23] Calculations were used to investigate the thermodynamic of the first Pt-Me protonolysis reaction with isolated surface hydroxyl in order to elucidate the ability of Zn/SiO_2 to stabilize the molecular organoplatinum sites. A cluster model of the SiO_2 support with six silica rings (Figure S3a) was used based on our previous computational study.[24] This cluster model was shown to be sufficient to model the amorphous silica. A single Zn^{2+} site was created on the silica cluster to mimic the anchoring sites of Zn/SiO_2 (Figure S3b). Two possible configurations of Zn/SiO_2 were considered: a 3-coordinate Zn^{2+} site (Zn/SiO_2-1, Figure S3b) and a 4-coordinate hydroxylated Zn^{2+} site (Zn/SiO_2-2, Figure S3c) to account for the interaction of Zn/SiO_2-1 with a water molecule. It is notable that the formation of Zn/SiO_2-2 from Zn/SiO_2-1 requires a 5.3 kcal/mol energy at room temperature, suggesting that Zn/SiO_2-1 is thermodynamically more stable and more likely to exist at room temperature. The bottom half of the clusters (11 O, 6 H and 6 Si atoms) were kept frozen during the geometry optimizations while the top half and the interacting molecules were allowed to relax.

Solid-state NMR Spectroscopy. All solid-state (SS) NMR experiments were performed on natural-abundance samples, using a Bruker AVANCE III 400 spectrometer, operated at 9.4 T, equipped with a 9.7 T gyrotron for dynamic nuclear polarization (DNP) measurements as well as 3.2-mm low-temperature magic-angle-spinning (MAS) probe. For DNP, the samples were first impregnated with a 16 mM solution of TEKPol in 1,1,2,2-tetrachloroethane (TCE), with natural ^{1}H abundance (for ^{195}Pt and ^{17}O measurements) or 99.6% deuterated (for ^{13}C measurements), and then packed into 3.2-mm sapphire rotors.[25] The MAS frequency was set to either 12.5 kHz (^{17}O, ^{195}Pt), 12 kHz (^{13}C), or 0 kHz (^{195}Pt, a static measurement) and the sample temperature was approximately -163 °C under MAS and -148 °C under the static condition.

The ^{1}H-^{17}O distance measurements were carried out using a DNP-enhanced ^{17}O{^{1}H} windowed-proton-detected local field (wPDLF)[26] technique with quadrupolar Carr Purcell Meiboom Gill (QCPMG)[27] acquisition scheme. The wPDLF sequence was used as previously published,[26, 28] with $wR18_2^5$ recoupling (50% window) for the distance measurement and $R18_1^7$ for PRESTO population transfer (PRESTO = phase-shifted recoupling effects a smooth transfer of order).[29] The ^{17}O central-transition-selective 90° and 180° pulses lasted 5 and 10 μs, respectively, and the QCPMG spikelet separation was set to 6.25 kHz. 800 scans were accumulated for each t_1 increment of a single recoupling block and a total of 20 increments were acquired.

The ^{13}C CPMAS spectrum of catalyst **1** was acquired using a CP (cross-polarzation) contact time of 250 μs; the ^{1}H and ^{13}C 90° pulses both lasted 3 μs and 4096 scans were accumulated using a relaxation delay of 1 s. Two ^{13}C{^{1}H} HETCOR spectra were acquired using contact times of 100 and 4000 μs. Frequency-switched Lee-Goldburg homonuclear decoupling[30] was applied in t_1 to improve the resolution and a total of 18 increments of 33 μs, each consisting of 1024 scans, were acquired using the States-TPPI method.

The DNP-enhanced ^{195}Pt spectra were acquired using the standard ^{195}Pt CPMAS and the static wideline BCP-WCPMG experiment, consisting of broadband adiabatic inversion ^{1}H-^{195}Pt CP (BRAIN-CP)[31], which incorporates wideband uniform rate and smooth truncation (WURST)[32] pulses for spin inversion and CPMG refocusing.[33] The ^{195}Pt CPMAS spectrum was acquired using a CP-echo sequence in which the contact time was set to 5 ms and the refocusing pulse lasted 9 μs. The ^{1}H excitation pulse lasted 2.75 μs and total of 3072 scans were accumulated with a 4 s recycle delay. The BCP-WCPMG spectrum was acquired using again a contact time of 5 ms during which a WURST adiabatic pulse sweeping over 250 kHz was applied to ^{195}Pt. For the WCPMG detection 50 μs WURST pulses sweeping over 500 kHz were used and the spikelet separation was set to 5 kHz. The ^{1}H excitation pulse lasted 2.75 μs and total of 2600 scans were accumulated with a 4 s recycle delay. In the case of the molecular precursor, only 64 scans were needed. Both the static and MAS spectra were simulated using WSolids.

X-ray Absorption Spectroscopy (XAS). X-ray absorption near edge structure (XANES) and extended X-ray absorption fine structure (EXAFS) measurements were carried out at the bending-magnet beamline of the Materials Research Collaborative Access Team (MR-CAT) at the Advanced Photon Source (APS) of Argonne National Laboratory. The X-ray beam was calibrated to the Pt L3- and Zn K-edges using Pt and Zn foils at 11.564 keV (Pt L3 edge) and 9.659 keV (Zn K edge). All XAS

measurements were taken in the transmission mode with ionization chambers optimized for the maximum current with linear response (~10^{10} photons detected/s). A cryogenically water cooled double-crystal Si(111) monochromator with a resolution better than 2.5 eV at 10 keV was used. With respect to sample preparation, the weight ratios of samples to boron nitride were first calculated to achieve an edge step corresponding around 1-1.5 total absorbance unit for all samples and standards. The samples were then mixed with boron nitride and finely ground using a mortar and pestle. 5-10 mg of the mixture was placed into a six-well sample holder where the radius of each well is around 2.0 mm. The sample was pressed as a pellet, completely blocking the well, such that the flow of gases could only pass through the pellet. The sample holder was then inserted into a quartz tube (1–in. OD, 10–in. length) which was centered at the furnace and sealed with Kapton windows by two Ultra-Torr fittings. For *in situ* XAS experiments, 50 mL/min of 3% H_2/He was introduced to the sample tube and the temperature of the furnace was increased to 135 and 200 °C. The EXAFS spectra for high-temperature-treated samples were taken after the reactor was cooled down to RT under the H_2 environment. Background removal and normalization procedures were carried out using the Athena software package (version 0.9.24) using standard methods. Standard procedures based on Artemis software were used to extract the EXAFS data. The coordination parameters were obtained by a least square fit in R-space of the nearest neighbour, k2-weighted Fourier transform data (Figure S7).

Catalytic Hydrogenation of 1,3-Butadiene. A 16-channel high-throughput fixed bed system (Flowrence® from Avantium) was used for the catalytic experiments. 10 to 80 mg catalyst was mixed with 100 mg Davisil Silica and loaded into a quartz reactor (2 mm ID, 30 mm length). For 1,3-butadiene hydrogenation, a total flowrate of 20.31 mL/min was used per reactor of which 18.75 mL/min 1% 1,3-butadiene/Ar, 0.56 mL/min H_2, and 1 mL/min He as internal standard. The temperatures tested were 50 to 200 °C (5 °C/min) with an increment of 25 °C. At each temperature, a gas sample was taken automatically, sequentially from reactor #1 to reactor #16, for gas chromatography analysis.

Catalytic Hydrogenation of Nitro-Aromatics. An automated synthesis platform (Core Module 3, CM3, Unchained Labs Inc.) that is located in a custom-built N_2-filled glovebox (MB 200B, MBraun) and a Screening Pressure Reactor (SPR, Unchained Labs Inc.) in Argonne National Laboratory's High-throughput Research Facility, were used for the high-throughput experiments. Matrices of experiments and protocols were designed in Library Studio while Automation Studio (LEA software) was used for running the protocols. Simultaneous testing of all the catalysts and controls were carried out in multi-well plates that can hold 48 2-mL glass vials per run. In every catalysis run, negative controls were implemented using the thermal sample and the metal-free silica. The solid catalysts were pre-reduced in 10% H_2/N_2 mixture at 135 ºC for 30 min. The CM3 performed solid and liquid dispensing. The catalysts were dispensed through disposable shaker vials (SV) with polytetrafluoroethylene (PTFE) hoppers and weighed using an automated balance (± 0.2 mg accuracy). 750 µL of a 0.25 M stock solutions of each of the substrates were used for the hydrogenation experiments. Each solution was dispensed using a Rainin dispense tool equipped with a disposable, 1-mL positive displacement tip (PDT), operated by the CM3. The multi-well plate with vials was then covered with a pin-hole Teflon gasket and a stainless steel pin-hole plate to ensure gas diffusion but to minimize cross-contamination between the vials. The multi-well plate was then transferred into a clam-shell reactor, which was sealed inside the glovebox. The clam-shell reactor was then taken out to the SPR, which is designed to carry out pressure reactions with heating and orbital shaking. Initially, the SPR was flushed with 500 mL/min H_2 for 15 min at room temperature, pressurized, and set to shake at 300 rpm. The reactor was then heated up slowly (1 ºC/min ramp rate) to 40 ºC. Under the given conditions, the pressure of the reactor reached 45 psi. After 24 h, the shaking was stopped, the reactor was cooled down to room temperature, and was flushed with 100 mL/min N_2 for 15 min. The clam-shell reactor was then brought back to the glovebox. Aliquots were then transferred into filter vials (Whatman Mini-UniPrep Syringeless Filter, 0.2 um) to separate the solid catalysts from the organic solution and protect the GC columns.

Nitro-Aromatic Hydrogenation with a Homogeneous Organoplatinum(IV) Catalyst. 0.5 mg of Pt precursor [(MeCp)$PtMe_3$] was used for determining whether the molecular analogue is also catalytically active. The following reaction conditions were used in the SPR (*vide supra*): 750 µL of a 0.25 M stock solution of nitrobenzene, 75 ºC, 45 psi H_2, 24 h. No conversion was observed.

Recycling Experiment. A series of catalyst recyclability tests were carried out with nitrobenzene as test substrate. Two samples of 30 mg of catalyst **2** were used with 0.75 mL of 0.25 M nitrobenzene in toluene. After the first reaction (75 °C, 200 psi H_2, 24 h), the supernatants were removed carefully and set aside for GC analyses. The "wet" catalysts were then rinsed with a fresh solution of nitrobenzene in toluene. This was repeated twice, before adding a fresh solution. Three consecutive runs were performed.

Leaching Test. 30 mg of catalyst **2** was used with 0.75 mL of 0.25 M nitrobenzene in toluene. The first reaction (75 °C, 200 psi H_2) was carried out for 1 h; then the supernatant was removed carefully and spilt into 2 samples, one for GC analyses and one for further reaction. The initial conversion after 1 h was 91%. The remaining supernatant was then exposed to 200 psi H_2 for 23 h at 75 °C.

Real-time Monitoring of the Reduction of Nitrobenzene. For kinetic measurements, the Optimization Screening Reactor (OSR, Unchained Labs Inc.) located in the N_2-filled glovebox, was used. It has 8 parallel batch reactors with independent temperature and pressure control and a common overhead stirring, with the capability of sampling during reaction. First, catalyst **2** (50, 100 or 200 mg) was loaded manually. Then, a 25 mL stock solution (either 0.125, 0.25 or 0.50 M nitrobenzene in toluene) with 1,3,5-trimethylbenzene as internal standard, was added, also manually. The rest of the procedure was controlled

Scheme 1. Solution-phase synthesis of highly dispersed organoplatinum(IV) sites on a Zn/SiO_2 support with (MeCp)$PtMe_3$ in toluene at room temperature (**1**) and hydrogenolysis of **1** to form **2** at 135 °C under an atmosphere of H_2.

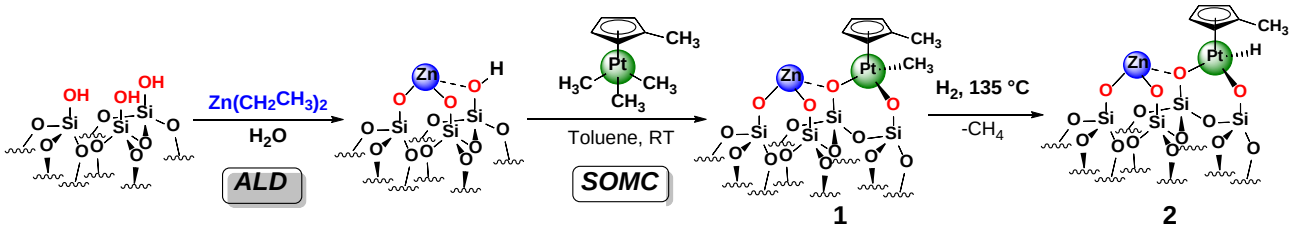

by the LEA software; the reactors were purged with N_2 twice and then heated to various temperatures (60, 75 or 90 ºC), flushed twice and pressurized with H_2 (UHP grade, oxygen and moisture trapped) up to various pressures (100, 200 or 300 psi). Stirring was set at 250 rpm, with a settling delay of 15 s prior to sampling to avoid carrying over catalyst powder. Automated sampling of 100 µL was performed at various times, and dispened into vials (Whatman Mini-UniPrep Syringeless Filter, 0.2 um), on a 48 well plate, preloaded with 100 µL of dodecane.

GC-MS and GC-FID Analyses. The compositions of the reaction mixtures were determined using a Trace GC Ultra Gas Chromatograph system equipped with a Tri Plus RSH autosampler, an ISQ MS detector, and a FID (Thermo Scientific). The column used for the MS detector was an Agilent J&W DB-5 column (30 m × 0.25 mm × 0.25µm film thickness) while the column used for the FID was an Agilent J&W DB-5MS column (30 m × 0.25 mm × 0.25µm film thickness). GC data were analyzed using the Thermo Xcalibur 2.2 SP1.48 software. The following method was used: a 0.5 µL split injection with a split ratio of 100 run under a constant gas flow of 1 mL/min. The oven temperature profile was as follows: initial temperature = 30 °C, hold for 10 minutes, ramp at 20 °C/min, final temperature = 250 °C.

Results and Discussion

Synthesis of the Supported Organoplatinum Catalyst. Organoplatinum(IV) sites were installed by solution-phase SOMC on high-surface-area SiO_2 modified via ALD[19-20] with Zn^{2+} anchoring sites (Scheme 1). Based on the Zn loading (10% w/w; 75% of a theoretical Zn^{2+} monolayer), the Zn/SiO_2 support contains both isolated Zn^{2+} sites and ZnO-rich areas (see NH_3-TPD trace in Figure S2). However, only surface hydroxyls associated with isolated Zn^{2+} have increased acidity, rendering the Zn/SiO_2 system more capable of stabilizing Pt^{4+} sites, relative to traditional SiO_2. Recent studies have shown that the O-H bond lengths of surface hydroxyl groups, as measured by DNP-enhanced $^{17}O\{^1H\}$ wPDLF-QCPMG experiments, correlate strongly with the Brønsted acidity of these groups.[28] Specifically, the more Brønsted acidic surfaces were found to have the longer average O-H bond lengths. Thus, in order to obtain an independent confirmation that the Zn/SiO_2 support is indeed more Brønsted acidic, $^{17}O\{^1H\}$ wPDLF-QCPMG spectrum was acquired and compared it with the untreated SiO_2 (Figure 1). As can be seen in Figure 1, the dipolar splitting for the Zn/SiO_2 material is *qualitatively* narrower, yielding the longer average O–H bond length of 1.034 ± 0.007 Å, compared to 1.022 ± 0.006 Å for the silica, which indeed corroborates higher Brønsted acidity for Zn/SiO_2.

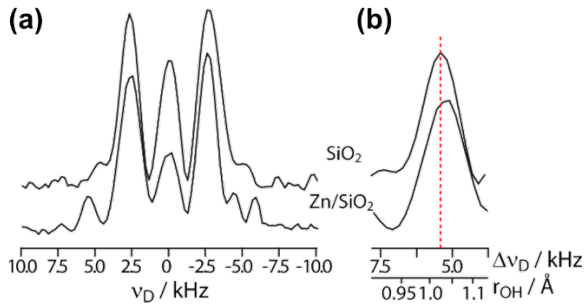

Figure 1. (a) Overlaid $^{17}O\{^1H\}$ wPDLF-QCPMG spectra of SiO_2 and Zn/SiO_2. (b) An enlarged view of the higher-frequency peak is shown on the right with the lower-frequency peak set to 0 Hz in order to highlight the splitting. A dashed red line marks the center of the peak in SiO_2 in order to ease the comparison of the two spectra.

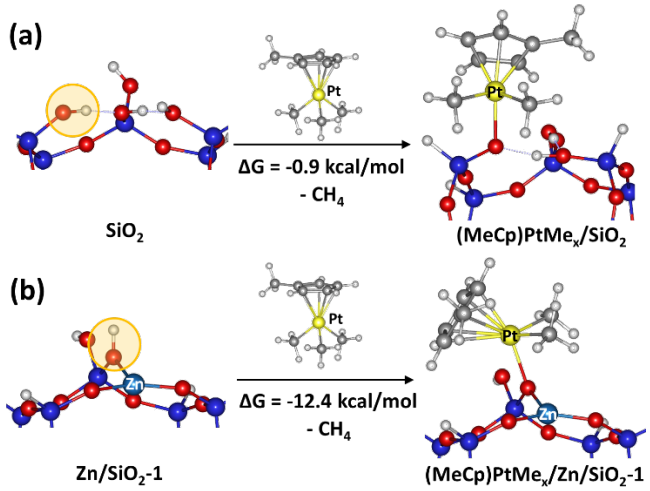

Figure 2. DFT calculations of the reaction free energies of $[(MeCp)PtMe_3]$ reacting with a hydroxyl group (highlighted) on (a) SiO_2 and (b) Zn/SiO_2 using cluster models of silica (method: B3LYP/CEP-31G). Blue, light blue, grey, light gray, yellow, and red spheres represent Si, Zn, C, H, Pt, and O, respectively.

Solution-phase organoplatination of Zn/SiO_2 with molecular $[(MeCp)PtMe_3]$ precursor in toluene at room temperature yields an air-stable (confirmed by XAS, *vide infra*), white, solid product [(MeCp)PtMe(0.2% w/w)/Zn(10% w/w)/SiO_2] (**1**). Under identical conditions, organoplatination of SiO_2 with $[(MeCp)PtMe_3]$ does not occur, thus, confirming the proposed effect of Zn^{2+} on surface hydroxyl acidity and reactivity. DFT calculations were performed to investigate the reactivity of SiO_2 and Zn/SiO_2 with the molecular precursor $[(MeCp)PtMe_3]$ at room temperature. These calculations illustrate the thermodynamics of the initial grafting reaction of the Pt complex onto the support. Computed thermodynamics of the first Pt-Me protonolysis event showed that the reaction between $[(MeCp)PtMe_3]$

and the hydroxyl groups on SiO_2 is likely to be reversible, with a reaction free energy of -0.9 kcal/mol at room temperature (Figure 2a). In comparison, the corresponding reaction with a bridge-coordinated hydroxyl group of the Zn/SiO_2 support is thermodynamically more favorable (ΔG = -12.4 kcal/mol, Figure 2b), presumably due to the increased acidity of the hydroxyl group (Brønsted acid site) bridging a Zn and a Si center. In addition, we also investigated the reactivity of a Zn(II)-bound hydroxyl group on Zn/SiO_2 (Zn/SiO_2-2 in Figure S3c), which is relatively less stable (5.3 kcal/mol higher) than Zn/SiO_2-1 (Figure 2b) at room temperature. The calculations indicated that the reactivity of Zn/SiO_2-2 with [(MeCp)PtMe$_3$] is consistently more favorable than SiO_2 (See Figure S4). These results support the experimental observations that at room temperature, solution-phase Pt deposition is more favorable on Zn/SiO_2 than on SiO_2.

Structural Characterization of the Supported Organoplatinum Catalyst. Results of a combination of solid-state characterization techniques (TPR-H_2, TEM imaging) and spectroscopic methods, including XAS, DNP-enhanced multinuclear SS NMR, DRIFTS and DRUV-Vis revealed that the Pt sites in **1** are predominantly at the tetravalent state, bound on dianionic siloxy sites, and are stabilized by anionic hydrocarbyl groups such as methylcyclopentadienyl and methyl ligands (Scheme 1). Previously reported Zn K-edge XAS studies of Zn deposition on SiO_2 via ALD[20] and strong electrostatic adsorption (SEA)[34] revealed the single-site nature of tri-coordinate Zn^{2+} centers on the surface (Figure S5, Table S1). Platinum L3-edge XAS (Figure 3) was employed to elucidate the electronic structure and coordination environment of Pt in **1**. XANES (Figure 3a) confirmed tetravalent state of the Pt centers based on the edge absorption energy at 11566.6 eV (the same value was obtained for tetravalent molecular precursor [(MeCp)PtMe$_3$]) and similar white line intensity. The EXAFS spectrum of **1** (Figure 3b and Table 1) proposed a Pt coordination very similar to that of [(MeCp)PtMe$_3$]: i) three coordination units at the Pt–O/C scattering path (2.02 ±0.02 Å) and ii) five coordination units at the MeCp-Pt bond distance (2.30 ±0.02 Å); the latter suggests that the MeCp-Pt moiety remains intact after the Zn/SiO_2 platination. EXAFS features corresponding to Pt-O-Zn moieties in **1** were not detected. Additionally, the EXAFS spectrum of **1** does not show higher shell scattering paths corresponding to Pt–O–Pt and Pt–Pt moieties, *indicative* of Pt mono-nuclearity (Figure 3b).

Solid-state ^{13}C and ^{195}Pt NMR spectroscopy was also employed to elucidate the structure of the Pt sites in **1**. Due to the low Pt loading, the application of DNP was necessary to obtain spectra within a reasonable time.[35] The DNP-enhanced ^{13}C CPMAS spectrum of **1** (Figure 4a) shows the expected resonances corresponding to the methylcyclopentadienyl ($\delta \sim$ 119, 98, and 88 for the Cp (A-C) and 13 ppm for the MeCp (D)) and Pt-Me ($\delta \sim$ -12 ppm (E)) ligands.[36] $^{13}C\{^1H\}$ HETCOR experiments were used to further confirm these assignments. As can clearly be seen in Figure 4a, when a short CP contact

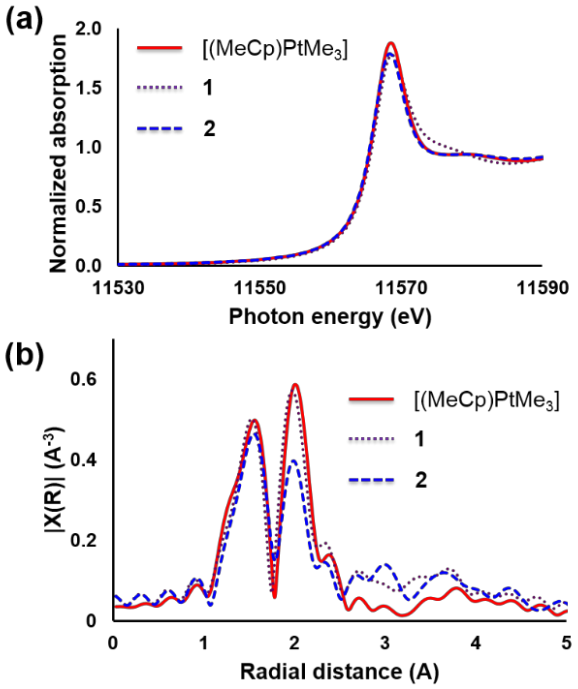

Figure 3. Pt L3-edge spectra: (a) XANES and (b) EXAFS spectra of pre-catalyst **1** (purple), pre-catalyst **1** treated with H_2 *in situ* at 135 °C (**2**, blue), and the molecular precursor [(MeCp)PtMe$_3$] (red).

Table 1. EXAFS fitting summary for **1**, **2**, and the molecular [(MeCp)PtMe$_3$] reference.[a]

Pt system	Path	CN	Bond Dist. (Å)	σ^2 (Å^2)[b]
[(MeCp)PtMe$_3$]	Pt-C_{Me}	3(set)	2.05(1)	0.0018
	Pt- Pt-C_{MeCp}	5(set)	2.31(1)	0.0053
1	Pt-C_{Me}/O	2.8(3)	2.02(1)	0.0018
	Pt-C_{MeCp}	5.0(6)	2.30(1)	0.0053
2	Pt-C_{Me}/O	2.7(3)	2.02(1)	0.0018
	Pt-C_{MeCp}	4.6(6)	2.32(1)	0.0053

[a]S_0^2 = 0.67, k-range = 3 – 14 Å^{-1}, R-range = 1.2 – 2.2 Å, k-weight = 2. [b]Debye-Waller factor.

time (τ_{CP} = 100 μs) is used, the correlations to the quaternary carbon are absent and only single-bond correlations can be observed. When the contact time is increased to 4 ms, however, a correlation between carbon A and the methyl protons of D canbe observed. Furthermore, an additional correlation between the methyl ligand (E) and the aromatic protons of the MeCp ring can be observed, confirming that both ligands are found within the same complex, in agreement with the proposed dominant structure for **1**. Note that deuterated TCE was used for these measurements and thus correlations to the solvent molecules are effectively quenched.[37]

Unfortunately, the ^{13}C spins from the MeCp ligand were found to have very short $T_{1\rho}$ relaxation times and thus no information regarding podality could be obtained from the ^{13}C spectra. The surface podality of the Pt(IV) sites could, however, be

verified via DNP-enhanced ^{195}Pt SSNMR.[38] ^{195}Pt chemical shifts are very sensitive to local bonding environment and span a range of 14000 ppm,[39] which should enable a clear distinction of the different coordination modes. It has been observed that substitution of a methyl ligand for a hydroxyl group shifts the resonance by *circa* 1600 ppm.[40] Given that the ^{195}Pt chemical shift of the molecular precursor [(MeCp)PtMe$_3$] is -5256 ppm,[41] a monopodal complex can be expected to have a chemical shift in the vicinity of -3656 ppm and a bipodal complex at around -2056 ppm. We have thus searched for the ^{195}Pt resonance using the BCP-WCPMG[33] experiment starting at -5500 ppm and increasing in frequency until a signal was detected. No signal could be found between -5500 ppm and -3000 ppm thus

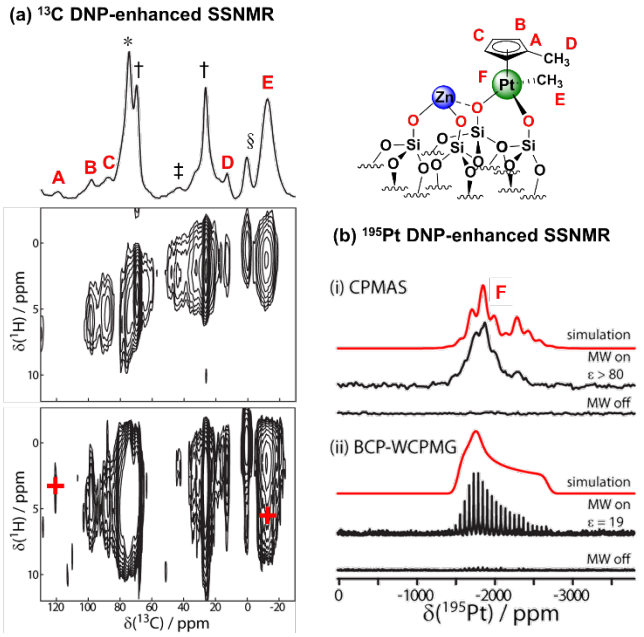

Figure 4. (a) DNP-enhanced ^{13}C CPMAS spectrum (top) and ^{13}C{^{1}H} HETCOR spectra (bottom) of **1**. The resonances from the complex are labeled A-E and identified on the structure shown; *: TCE, †: THF, ‡ Si-OMe, §: Si-Me. Two HETCOR spectra are shown with contact times of 100 and 4000 μs; the former showing mainly single-bond correlations while the latter one also features correlations between quaternary carbon A and the methyl protons as well as a correlation between the methyl ligand and the Cp ring protons (both indicated by red plus signs). (b) DNP-enhanced ^{195}Pt spectra of **1** obtained using CPMAS (i) and BCP-WCPMG (ii). In both cases the spectra acquired with and without microwave irradiation are shown, as indicated on the Figure, with the simulation overlaid in red.[42]

demonstrating that the quantity of physisorbed and/or monopodal complexes is negligible. A strong signal was, however, detected around -2000 ppm (Figure 4b), with a characteristic chemical shift anisotropy (CSA) lineshape (δ_{iso} = -2000 ppm, Ω = 1050 ppm, κ = 0.6). The small CSA is consistent with a pseudo-tetrahedral coordination environment and this resonance's isotropic chemical shift of -2000 ppm is exactly as expected from the bipodal Pt complex **1**, *vide supra*. We have additionally acquired a ^{195}Pt BCP-WCPMG spectrum of the molecular precursor which also featured a very small CSA, in agreement with what was observed in the surface-supported complex (Figure S8).

The DRIFTS, DRUV-Vis, and TPR-H$_2$ measurements confirmed the presence of organic moieties in **1**. Infrared absorptions at 3010 and 2930 cm^{-1} were observed, attributable to methyl and cyclopentadienyl C–H bonds, respectively (Figure S10). The DRUV-Vis spectrum of **1** (Figure S11) exhibits a strong absorption at 230 nm compared to the Zn/SiO$_2$ support. This is likely due to ligand to metal charge transfer (LMCT) transition of the surface-supported (methylcyclopentadienyl) methylplatinum(IV) sites. On the other hand, Pt nanoparticles exhibit a broad absorption band between 350-450 nm.[43] These well-differentiated features indicate that the electronic structure of the Pt species in **1** and PtZn nanoparticles are readily distinguishable, with the former having isolated and dispersed Pt and Zn sites present. The TPR-H$_2$ experiments showed two hydrogen consumption events at 135 °C and 157 °C, the first of which occurs with observable generation of CH$_4$ presumably from the hydrogenolysis of Pt–Me groups (Figure 5).

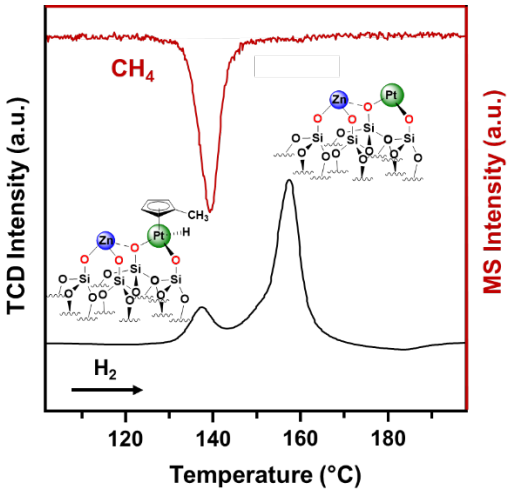

Figure 5. Temperature-programmed reduction of **1** showing H$_2$ consumption events occurring at 135 °C and 157 °C. Generation of CH$_4$ (upper plot) was observed during the H$_2$ consumption at 135 °C.

In situ XANES experiments of **1** with H$_2$ treatment at 135 °C occurs without an observable change in the initial Pt^{4+} oxidation state (XANES edge energy = 11566.4 eV), suggesting the likely formation of supported (MeCp)PtH/Zn/SiO$_2$ species (**2**, Scheme 1). On the other hand, the hydrogen consumption event at 157 °C resulted in the formation of a Pt^{2+} species (**4**, XANES edge absorption energy = 11564.6 eV, Figure S6), with an observable reduction of C–H stretching frequencies in the DRIFTS spectrum (Figure S10), attributable to the hydrogenolysis of the Pt–(MeCp) moiety. The two hydrogen consumption events, give distinct supported Pt species (Figure 5) with well differentiated catalytic behavior *(vide infra)*. The formation of a supported Pt–H species (**2**) was proposed via *in situ* DRIFTS experiments, where a broad vibration feature at 1950-2050 cm^{-1} was detected upon exposure of **1** to a pure H$_2$ feed from 50 to 150 °C (Figure 6). Note that the observed range of Pt–H vibrational frequencies is consistent with reported infrared frequencies for molecular and supported Pt–H species;[44] however formation of other organoplatinum species cannot be ruled out.

Similar experiments performed using pure D_2 resulted in a Pt–D formation, observed at 1565 cm^{-1} (Figure S13), consistent with literature values for a Pt–D species and

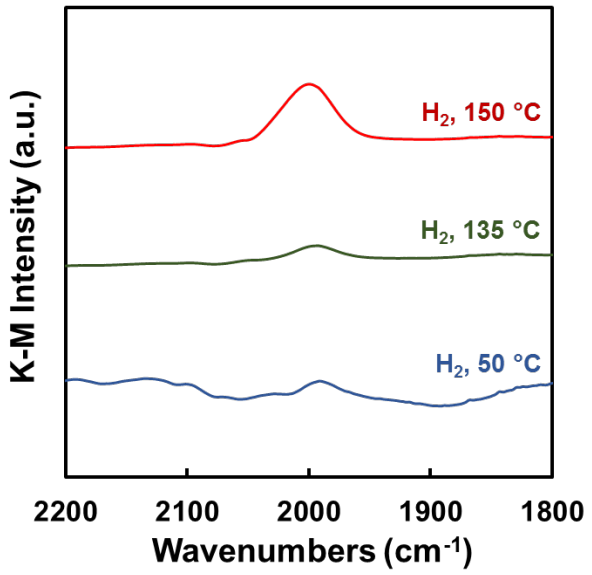

Figure 6. *In situ* DRIFTS (2200-1800 cm^{-1} region) experiments with **1** under pure H_2 atmosphere. The DRIFTS measurements were carried out over a range of temperatures (from 50 to 150 °C).

the DFT-predicted frequency for a terminal platinum(IV) deuteride on a Zn/SiO_2 support.[44a-c, 44e] A weak vibrational feature at 1950-2050 cm^{-1}, attributable to a possible Pt-H species, was also observed under a D_2 atmosphere presumably due to H-D exchange with surface O–H sites and generation of molecular H–D *in situ*.[45] Exposure of supported Pt–H species to air resulted in the disappearance of such feature (Figure S14). The formation of supported Pt–H was not observed during *ex situ* ^1H SS NMR experiments, indicating that the formation of the supported Pt–H species may be reversible and only favored under an atmosphere of H_2.

Finally, the FTIR-CO chemisorption, an established methodology to structurally characterize Pt species on surfaces,[46] was exploited to confirm the dispersity of Pt and the absence of clusters in **1**. Exposure of **1** to CO at room temperature revealed the presence of isolated, Pt^{4+} sites based on the IR stretching frequencies observed at 2135 and 2145 cm^{-1}, which disappear upon flushing with a pure He feed, attributable to labile, terminally bound carbonyl ligands (Figure 7).[10, 47] Treatment of **1** with H_2 at 100 and 200 °C did not result in observable formation of Pt aggregates, as evidenced by the terminal CO absorptions at 2080 cm^{-1}, characteristic of isolated Pt sites.[47] Since no reduction event was observed in the *in situ* XAS studies of the H_2-treatment of **1** at 135 °C, the observed non-reversible CO binding sites in **2** is proposed to be mainly due to a combination of electronic (decrease in electrophilicity of the Pt(IV)-H sites[48]) and steric (replacement of the bulkier platinum-bound methyl groups with a hydride) effects. Carbonyl stretching at lower frequencies characteristic of the bridging CO species were not detected, consistent with the Pt monodispersity initially observed in the EXAFS spectrum. The spectroscopic evidence for Pt monodispersity (Table 2) is also consistent with results of high-resolution TEM imaging of **1**, where Pt agglomerates were not observed (Figure 8a).

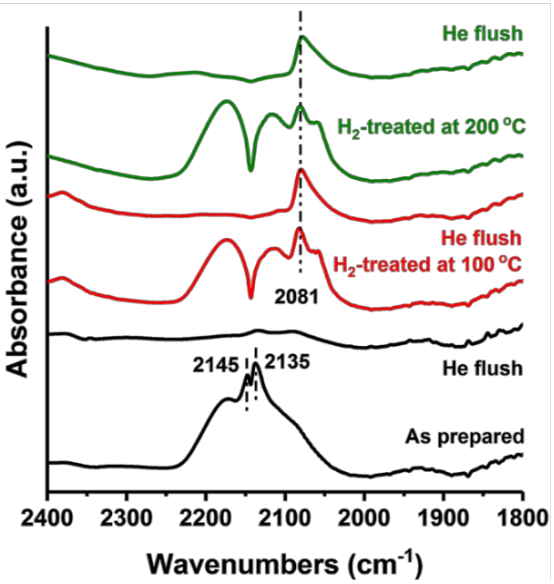

Figure 7. Figure 7. IR-CO chemisorption spectrum of **1** and **2** under various treatment conditions. The spectra for CO were collected after H_2 treatment at 100 and 200 °C. All the spectra were background subtracted using the spectra collected before CO exposure at each temperature.

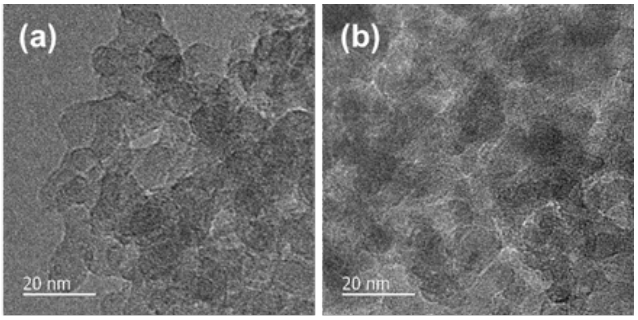

Figure 8. TEM images of the (a) as-prepared **1**, and (b) **1** treated with H_2 at 135 °C (**2**).

Table 2. Characterization Experiments and Interpretation of Zn/SiO_2, (MeCp)PtMe/Zn/SiO_2 (**1**), and (MeCp)PtH/Zn/SiO_2 (**2**).

System	Experiments	Observation	Interpretations
Zn/SiO_2	NH_3-TPD	New NH_3 desorption at 207 °C	Acid sites
	DNP- enhanced $^{17}O\{^1H\}$ wPDLF	Increased average O–H bond length of 1.034 ± 0.007 Å	
	Zn K-edge XAS	Tri-coordinate Zn^{2+}	Isolated anchoring-sites
(MeCp)PtMe/Zn/SiO_2 (1)	ICP-MS	0.2 % w/w Pt	Low metal loading
	Computed thermodynamics of the first Pt–Me protonoly-sis	ΔG = -12.4 kcal/mol	Thermodynamically favorable grafting
	Pt L3-edge XAS	XANES edge absorption energy at 11566.6 eV	Pt^{4+}
		EXAFS spectrum similar to that of the molecular [(MeCp)$PtMe_3$] precursor	Tetrahedral Pt center stabilized by divalent siloxy sites, anionic MeCp, and Me ligands
	DNP-enhanced ^{13}C SSNMR	δ ~ 119, 98, and 88 for Cp, 13 ppm for MeCp, and -12 ppm for PtMe	[(MeCp)PtMe] fragment is grafted onto Zn/SiO_2
	DNP-enhanced ^{195}Pt SSNMR	δ ~ –2000 ppm	Pseudo-tetrahedral bipodal Pt complex
	DRUV-Vis	Absorption at 230 nm (LMCT)	Isolated Pt atom
	DRIFTS CO chemisorption	Stretching frequency Pt-CO 2135 and 2145 cm^{-1}	Isolated Pt atom
	High-resolution TEM imaging	No observable NPs or Pt cluster	Isolated Pt atom
	TPR-H_2	H_2 consumption at 135 °C	Formation of Pt^{4+}-H
		H_2 consumption at 158 °C	Reduction to Pt^{2+}
(MeCp)PtH/Zn/SiO_2 (2)	Pt L3-edge XAS	XANES edge absorption energy at 11566.4 eV	Pt^{4+}
		EXAFS spectrum similar to **1**	Tetrahedral Pt center stabilized by divalent siloxy sites, anionic MeCp, and H ligands
	DRIFTS H_2	Broad stretching frequency at 1950-2050 cm^{-1}	Formation of Pt-H
	DRIFTS D_2	Stretching frequency at 1565 cm^{-1}	Formation of Pt-D
	DRIFTS CO chemisorption	Stretching frequency Pt-CO at 2080 cm^{-1}	Isolated Pt atom
	High-resolution TEM imaging	No observable NPs or Pt cluster	Isolated Pt atom

Catalyst Evaluation. ***Catalytic hydrogenation of dienes to butenes*.** The H_2 consumption events observed for **1** in the TPR-H_2 and XANES experiments generate distinct Pt species with potentially different reactivity. Activation of **1** with H_2 at temperatures below 100 °C, insufficient conditions to form the active species **2**, did not result in any observable 1,3-butadiene hydrogenation activity. On the other hand, activation at temperatures (>100 °C) high enough for Pt–Me hydrogenolysis results in the catalytically active material **2** (Scheme 1) that semi-hydrogenates 1,3-butadiene to a mixture of butenes, with 1-butene being the major hydrogenation product, under plug-flow reactor conditions (Figure 9). Activation of **1** to **2** over a range of temperatures (100 to 150 °C; GHSV = 3490 h^{-1}) afforded 14 to 44% butadiene conversion, respectively, with the total selectivity to butenes (91-95%) largely unchanged regardless of the conversion level. The high mono-olefin selectivity is a strong

indication of stable catalyst selectivity. Note that under identical catalytic conditions (100 to 150 °C), 1,3-butadiene hydrogenation with the corresponding PtZn nanoparticle catalyst (**3**) synthesized via calcination of **1** in air at 550 °C results in complete conversion to *n*-butane, confirming that the selective semi-hydrogenation to butenes observed with **2** is not due to nanoparticle catalysis. Moreover, 1,3-butadiene hydrogenation with catalyst **1** activated at temperature > 150 °C (**4**) resulted in complete conversion along with loss of butene selectivity, suggesting possible formation of PtZn nanoparticles (*vide infra*).

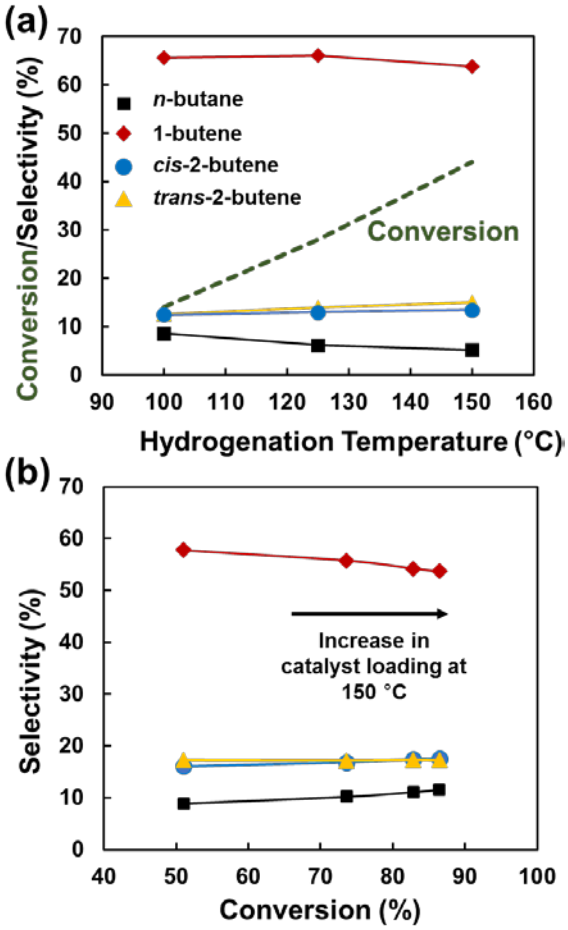

Figure 9. (a) Mild-condition pre-activation of **1** (100 to 150 °C), to afford catalyst **2**, results in chemoselective hydrogenation of 1,3-butadiene to a mixture mainly composed of butenes (91-95% selectivity). The formation of the secondary hydrogenation product, *n*-butane, is minimal at different hydrogenation temperatures and conversion levels. (b) Isothermal hydrogenation of 1,3-butadiene at 150 °C with varying catalyst amounts (10, 20, 40, and 80). The overall selectivity to butenes is largely unaffected by increased conversion.

Near quantitative conversion of 1,3-butadiene (86% at 150 °C; Figure 9b) were observed with increase in catalyst loading and slower flow rates (GHSV = 3490 h^{-1}), with the selectivity to butenes remaining high at 89%. TEM imaging of the H_2- treated catalyst indicates that no sintering occurs upon reduction of **1** at 135 °C (Figure 8b), suggesting that highly dispersed Pt sites are responsible for the observed hydrogenation activity. Additionally, under the same reaction conditions, the non-platinated support Zn/SiO_2 is unreactive under the given conditions, confirming that Pt is mainly responsible for the observed catalytic hydrogenation activity.

The catalyst preactivation temperature was observed to affect the resulting activity and selectivity. H_2-activation at 135 °C gives the more selective catalyst, while activation at 200 °C yields a non-selective material. Variable-temperature DRIFTS experiments (Figure S10) revealed that preactivation at higher temperatures (>150 °C) reductively cleaves the MeCp–Pt group to form a Pt^{2+} (**4**, XANES edge energy = 11564.6 eV, Figure S6) species with lower chemoselectivity for nitro-aromatic reduction. The removal of the MeCp group at 200 °C is also observed using solid state ^{1}H NMR (Figure S9). This suggests that electronic and steric contributions from the MeCp ligand are vital to the chemoselectivity.

Nitro-aromatic reduction. The observed selective semi-hydrogenation of dienes to mono-olefins indicates the potential utility of **2** for chemoselective hydrogenation of nitro-aromatic substrates functionalized with hydrogenation-sensitive groups. Single-atom catalysts[49] are, by far, the most studied supported systems for chemoselective hydrogenation of nitro-aromatics, while supported surface organometallic catalysts, to the best of our knowledge, have never been reported for this chemical transformation. Both systems take advantage of Pt site isolation and the postulate that nitro groups are more reactive to isolated Pt sites compared to other reducible group(s) (e.g., C=C and C=O bonds) which are more sensitive to the size/nuclearity of the active metal. Chemoselective hydrogenation of 3-nitrostyrene is particularly challenging as C=C bonds are generally highly reactive to Pt sites. Catalyst **2** hydrogenates 3-nitrostyrene to 3-aminostyrene as the main product (Table 3, entry 1; 46% conversion, 79% selective) at 0.04 mol% Pt loading, 40 °C in toluene under 50 psi H_2. Under the same reaction conditions, catalyst **3** exhibits expected non-selective nanoparticle-like reactivity (37% selective to 3-aminostyrene at 53% conversion). The observed higher selectivity of **2** to 3-aminostyrene is comparable to the selectivities reported by Wei and coworkers for single-atom and pseudo-single-atom Pt sites on Fe_yO_x support.[10] Catalyst **2** exhibits higher activity and chemoselectivity, and hydrogenates a wider scope of functionalized nitro-aromatic substrates compared to the supported PtZn nanoparticle system (**3**). The well-differentiated selectivity between catalysts **2** and **3** is a confirmation that site-isolated organoplatinum sites in **2** are catalytically responsible for the observed reactivity. Catalyst **2** was evaluated for the reduction of a range of nitro-aromatics functionalized with reactive (olefin, carbonyl, nitrile, halogens) groups under identical conditions: 40 °C, 50 psi H_2, 24 h (Table 3). Quantitative conversion of isomeric nitro-benzaldehydes (entries 3-4) was observed with complete tolerance of the aldehyde moiety. 2-nitrobenzaldehyde hydrogenation proceeds faster than 4-nitrobenzaldehyde, presumably due to the directing effect of the adjacent electron-withdrawing aldehyde group in the ortho-substituted substrate. Additionally, the high chemoselectivity to 2-aminobenzaldehyde confirms the ability of **2** to discriminate between adjacent reducible moieties, which is rarely observed with Pt nanoparticles.[50] Hydrogenations with comparable rates and selectivities were observed in the case of isomeric nitro-styrenes (entries 1-2).

Table 3. Substrate scope study using catalyst **2**: hydrogenation of nitro-aromatics (0.25 M in toluene) functionalized with reducible functionalities at 40 °C, 50 psi H_2, 24 h.[a]

Entry	Substrate	Pt loading (mol %)	Conversion (%)	Product	Selectivity (%)
1	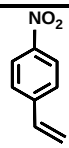	0.04 0.08 0.04[b]	46 67 >99	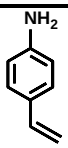	79 75 0[c]
2	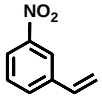	0.04	55		84
3	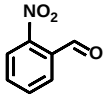	0.04	>99	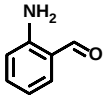	>99
4	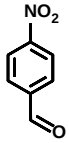	0.04 0.08 0.04[b]	46 85 >99	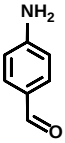	>99 >99 >99[c]
5	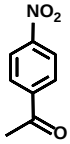	0.04 0.04[b]	81 >99	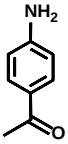	>99 >99
6	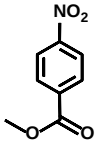	0.04 0.08 0.04[b]	53 74 >99	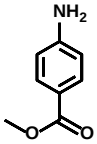	>99 >99 >99[c]
7	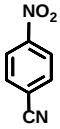	0.04 0.04[b]	46 >99	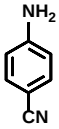	>99 >99
8		0.04 0.04[b]	53 >99		>99 70[d]
9		0.04	>99		>99

[a]Reaction conversions are based on measured GC concentrations. [b]The reaction was carried out at 75 °C. [c]4-ethylaniline was formed as the main product. [d]Dimerized anilines were detected as minor products.

On the other hand, modest conversions were observed for nitro-aromatics with polar, hydrogenation-sensitive groups (entries 5-8). Quantitative conversions were achieved at 75 °C, with complete tolerance of other hydrogenation-sensitive moieties such as aldehydes, ketones, esters, nitriles and chlorides. In general, the selectivity levels observed are superior to other reported supported PtZn catalysts for nitro-aromatic reduction.[18c,20]

Nitrobenzene is not as reactive as nitro-aromatics functionalized with electron-withdrawing groups, suggesting that electron-deficient nitro-aromatics are less reactive; hydrogenation to aniline was only observed at higher temperatures (75 °C, entry 9). Real-time monitoring of the reduction of nitrobenzene to aniline showed no formation of partial hydrogenation (hydroxyl-amines) and secondary products (e.g., dimerized products). A turnover frequency value of 809 ± 8 h^{-1} was observed at 10% nitrobenzene conversion (Figure S15). A three-cycle recyclability test was carried out under the nitrobenzene reduction conditions described above and confirmed that the catalyst is recyclable without any observable loss of catalytic activity and selectivity. Filtration of the reaction mixture to isolate the catalyst at 91% conversion and retesting of the liquid phase revealed that catalytically active, freely soluble Pt species do not leach into solution. This is consistent with the observation that the molecular precursor [(MeCp)$PtMe_3$] is catalytically inactive under the given nitro-aromatic hydrogenation conditions, ultimately confirming that supported (MeCp)Pt-H on Zn(II)-modified SiO_2 sites are responsible for the observed selective catalytic reaction. Importantly, the stability of the supported organoplatinum(IV) after catalysis was determined via DRIFT (Figure S17) which confirmed the presence of the CpMe ligand. In addition, negligible sintering of the Pt sites on Zn/SiO_2 was observed based on TEM (Figure S18) and PXRD (Figure S19) characterization of the spent catalyst.

Effect of loading of anchoring sites. The effect of the Zn^{2+} concentration was also investigated; surface saturation of SiO_2 with Zn^{2+} (10% w/w; 75% of a theoretical Zn^{2+} monolayer) gives the most active and selective catalyst at identical Pt loadings. Lower Zn^{2+} loadings resulted in observable Pt aggregation in the TEM image, forming crystalline ensembles that are less active and selective to 3-aminostyrene (Figure S15). The agglomeration of Pt on low-Zn^{2+} supports presumably arises from the presence of bare SiO_2 surface sites where Pt migration and sintering occur more easily. Surface saturation of SiO_2 with Zn^{2+} sites confirms our hypothesis on the positive effect of Zn^{2+} anchoring sites on Pt stability. In addition, the deposition methods and dispersion of Zn^{2+} sites on SiO_2 were observed to affect the dispersion of Pt sites and, in turn, the catalyst chemoselectivity. The Pt catalysts deposited on ALD-synthesized Zn(10%)/SiO_2 with monodispersed Zn^{2+} sites, showed superior performance compared to the corresponding Zn(10%)/SiO_2 support prepared by SEA. The presence of monomeric and oligomeric Zn sites on the Zn/$SiO_{2\text{-SEA}}$ was confirmed by DRUV-Vis spectroscopy (Figure S12).

Conclusions

The stabilization of isolated platinum sites on weakly interacting, high-surface-area oxides supports, such as silica, has been a major challenge in the development of chemoselective surface-supported Pt catalysts. Due to the weak Pt–support interaction, most synthetic protocols for Pt deposition on SiO_2 result in a distribution of sites, compromising catalytic selectivity. This work successfully demonstrated that room-temperature grafting of isolated organoplatinum(IV) catalyst can be achieved using a modified silica support, equipped with Lewis acid anchoring sites such as Zn^{2+}. The use of ALD was critical in enforcing uniform distribution of cationic zinc anchoring sites; traditional Zn deposition techniques, such as SEA and hydrothermal protocols, are less effective in dispersing zinc due to agglomeration, particularly at surface saturation. The resulting

surface-supported organoplatinum(IV) sites were fully characterized using a combination of *ex situ* and *in situ* spectroscopic techniques, including XAS, DRUV-Vis, DRIFTS, DNP-enhanced SSNMR (^{1}H, ^{13}C, ^{17}O, ^{195}Pt), TPR-H_2 and TEM. The cationic Zn anchoring sites stabilize high-valent oxidation state metals (i.e., Pt^{4+}), promote *in situ* formation of a probable metal-hydride, and prevent sintering and catalyst deactivation. Supported organoplatinum species are chemoselective catalysts for the semi-hydrogenation of 1,3-butadiene to a mixture of butenes and reduction of functionalized nitro-aromatic with excellent tolerance of sensitive functional groups, such as olefins, carbonyls, nitriles, and halogens.

In summary, a general strategy for the modification of high surface area oxide supports, such as silica, with cationic Zn anchoring sites via ALD afforded novel catalyst support with tunable acidic and electronic properties. This catalyst design strategy provides a potentially general design principle for the rational development of new classes of mono- and multimetallic selective catalysts. Further studies are ongoing to explore and demonstrate the generality of this catalyst design strategy and synthetic approach. In particular, Lewis acids and/or redox-active cationic anchoring sites, such as Al^{3+}, Ga^{3+} and Ce^{4+}, will be employed in the development of a series of surface-supported organoplatinum(IV) catalysts, which will be fully characterized, and evaluated for the chemoselective hydrogenation of dienes and nitro-aromatics (Table S2).

ASSOCIATED CONTENT

Supporting Information. This material is available free of charge via the Internet at http://pubs.acs.org.

Details of the synthesis of Zn/SiO_2 support, NH_3-TPD plot, additional DFT calculations and coordinates, additional XAS spectra, additional DRIFTS data, DRUV-Vis data, additional DNP data, conversion vs time plot of nitrobenzene hydrogenation, additional TEM images, PXRD and DRIFT spectra of the spent catalyst, scoping of platinum anchoring sites/promoters on SiO_2.

AUTHOR INFORMATION

Corresponding Authors

M. Delferro (delferro@anl.gov), C. Stair (pstair@northwestern.edu), J. Camacho-Bunquin (jeffrey.c.bunquin@exxonmobil.com).

Notes

The authors declare no competing financial interest.

ACKNOWLEDGMENT

This work was supported by the U.S. Department of Energy (DOE), Office of Basic Energy Sciences, Division of Chemical Sciences, Geosciences, and Biosciences, under Contract DE-AC02-06CH11357 (Argonne National Laboratory) and DE-AC02-07CH11358 (Ames Laboratory). The calculations were performed using the computational resources provided by the Laboratory Computing Resource Center (LCRC) at Argonne and National Energy Research Scientific Computing (NERSC) Center. Use of the Advanced Photon Source is supported by the U.S. Department of Energy, Office of Science, and Office of the Basic Energy Sciences, under Contract DE-AC-02-06CH11357. MRCAT operations are supported by the Department of Energy and the MRCAT member institutions. Use of the TEM at the Center for Nanoscale Materials at Argonne National Laboratory is supported by the U.S. Department of Energy, Office of Science, Office of Basic Energy Sciences, under Contract DE-AC02-06CH11357. Partial support for F.P. was through a Spedding Fellowship funded by the Laboratory Directed Research and Development (LDRD) program at the Ames Laboratory. F. P. thanks NSERC and the Government of Canada for a Banting Postdoctoral Fellowship. We thank Dr. A. P. Sattelberger for helpful discussion.

References

1. (a) Monguchi, Y.; Ichikawa, T.; Sajiki, H. *Chem. Pharm. Bull.* **2017**, *65*, 2-9; (b) Virtanen, P.; Salminen, E.; Maki-Arvela, P.; Mikkola, J.-P. In *Selective hydrogenation for fine chemical synthesis*, Wiley-VCH Verlag GmbH & Co. KGaA: 2014; pp 251-262; (c) Thomas, S. P.; Greenhalgh, M. D. In *Heterogeneous hydrogenation of C=C and C≡C bonds*, Elsevier B.V.: 2014; pp 564-604; (d) Blaser, H.-U.; Steiner, H.; Studer, M. *ChemCatChem* **2009**, *1*, 210-221.
2. Suchy, M.; Winternitz, P.; Zeller, M. *Catal. Today* **1997**, *37*, 121-136.
3. Yang, X.-J.; Chen, B.; Zheng, L.-Q.; Wu, L.-Z.; Tung, C.-H. *Green Chem.* **2014**, *16*, 1082-1086.
4. (a) Imamura, K.; Hashimoto, K.; Kominami, H. *Chem. Commun.* **2012**, *48*, 4356-4358; (b) Corma, A.; Serna, P. *Science* **2006**, *313*, 332-334; (c) Blaser, H.-U.; Studer, M. *Appl. Catal. A* **1999**, *189*, 191-204.
5. Herkes, F. E., *Catalysis of organic reactions*. CRC Press: 1998; Vol. 75.
6. Serna, P.; Concepción, P.; Corma, A. *J. Catal.* **2009**, *265*, 19-25.
7. Corma, A.; Serna, P.; Concepción, P.; Calvino, J. J. *J. Am. Chem. Soc* **2008**, *130*, 8748-8753.
8. Pang, H.; Gallou, F.; Sohn, H.; Camacho-Bunquin, J.; Delferro, M.; Lipshutz, B. H. *Green Chem.* **2018**, *20*, 130-135.
9. Serna, P.; Corma, A. *ACS Catal.* **2015**, *5*, 7114-7121.
10. Wei, H.; Liu, X.; Wang, A.; Zhang, L.; Qiao, B.; Yang, X.; Huang, Y.; Miao, S.; Liu, J.; Zhang, T. *Nat. Commun.* **2014**, *5*, 5634.
11. (a) Coperet, C.; Estes, D. P.; Larmier, K.; Searles, K. *Chem. Rev.* **2016**, *116*, 8463-8505; (b) Copéret, C.; Comas-Vives, A.; Conley, M. P.; Estes, D. P.; Fedorov, A.; Mougel, V.; Nagae, H.; Núñez-Zarur, F.; Zhizhko, P. A. *Chem. Rev.* **2016**, *116*, 323-421; (c) Conley, M. P.; Coperet, C. *Top. Catal.* **2014**, *57*, 843-851; (d) Coperet, C. *Chem. Rev.* **2010**, *110*, 656-680; (e) Copéret, C.; Chabanas, M.; Petroff Saint-Arroman, R.; Basset, J.-M. *Angew. Chem. Int. Ed.* **2003**, *42*, 156-181.
12. (a) Pelletier, J. D. A.; Basset, J.-M. *Acc. Chem. Res.* **2016**, *49*, 664-677; (b) Basset, J.-M.; Coperet, C.; Soulivong, D.; Taoufik, M.; Thivolle, C. J. *Acc. Chem. Res.* **2010**, *43*, 323-334; (c) Basset, J. M.; Ugo, R. In *On the origins and development of "surface organometallic chemistry"*, Wiley-VCH Verlag GmbH & Co. KGaA: 2009; pp 1-21; (d) Lefebvre, F.; Basset, J. M. *J. Mol. Catal. A: Chem.* **1999**, *146*, 3-12.
13. (a) Stalzer, M. M.; Delferro, M.; Marks, T. J. *Catal. Lett.* **2015**, *145*, 3-14; (b) Wegener, S. L.; Marks, T. J.; Stair, P. C. *Acc. Chem. Res.* **2012**, *45*, 206-214; (c) Marks, T. J. *Acc. Chem. Res.* **1992**, *25*, 57-65.
14. (a) Sohn, H.; Camacho-Bunquin, J.; Langeslay, R. R.; Ignacio-de Leon, P. A.; Niklas, J.; Poluektov, O. G.; Liu, C.; Connell, J. G.; Yang, D.; Kropf, J.; Kim, H.; Stair, P. C.; Ferrandon, M.; Delferro, M. *Chem. Commun.* **2017**, *53*, 7325-7328; (b) Lohr, T. L.; Mouat, A.; Schweitzer, N. M.; Stair, P. C.; Delferro, M.; Marks, T. *Energ. Environ. Sci.* ***2017***, *10, 1558-1562;* (c) Camacho-Bunquin, J.; Ferrandon, M.; Das, U.; Dogan, F.; Liu, C.; Larsen, C.; Platero-Prats, A. E.; Curtiss, L. A.; Hock, A. S.; Miller, J. T.; Nguyen, S. T.; Marshall, C. L.; Delferro, M.; Stair, P. C. *ACS Catal.* **2017**, *7*, 689-694; (d) Stalzer, M. M.; Nicholas, C. P.; Bhattacharyya, A.; Motta, A.; Delferro, M.; Marks, T. J. *Angew. Chem., Int. Ed.* **2016**,

55, 5263-5267; (e) Mouat, A. R.; Lohr, T. L.; Wegener, E. C.; Miller, J. T.; Delferro, M.; Stair, P. C.; Marks, T. J. *ACS Catal.* **2016**, *6*, 6762-6769; (f) Liu, S.; Tan, J. M.; Gulec, A.; Schweitzer, N. M.; Delferro, M.; Marks, L. D.; Stair, P. C.; Marks, T. J. *ACS Catal.* **2016**, *6*, 8380-8388; (g) Gu, W.; Stalzer, M. M.; Nicholas, C. P.; Bhattacharyya, A.; Motta, A.; Gallagher, J. R.; Zhang, G.; Miller, J. T.; Kobayashi, T.; Pruski, M.; Delferro, M.; Marks, T. J. *J. Am. Chem. Soc.* **2015**, *137*, 6770-6780; (h) Williams, L. A.; Guo, N.; Motta, A.; Delferro, M.; Fragala, I. L.; Miller, J. T.; Marks, T. J. *Proc. Natl. Acad. Sci. U. S. A.* **2013**, *110*, 413-418.

15. (a) Brown, C.; Lita, A.; Tao, Y.; Peek, N.; Crosswhite, M.; Mileham, M.; Krzystek, J.; Achey, R.; Fu, R.; Bindra, J. K.; Polinski, M.; Wang, Y.; van de Burgt, L. J.; Jeffcoat, D.; Profeta, S.; Stiegman, A. E.; Scott, S. L. *ACS Catal.* **2017**, *7*, 7442-7455; (b) Gallo, A.; Fong, A.; Szeto, K. C.; Rieb, J.; Delevoye, L.; Gauvin, R. M.; Taoufik, M.; Peters, B.; Scott, S. L. *J. Am. Chem. Soc.* **2016**, *138*, 12935-12947; (c) Fong, A.; Peters, B.; Scott, S. L. *ACS Catal.* **2016**, *6*, 6073-6085; (d) Szeto, K. C.; Gallo, A.; Hernandez-Morejudo, S.; Olsbye, U.; De Mallmann, A.; Lefebvre, F.; Gauvin, R. M.; Delevoye, L.; Scott, S. L.; Taoufik, M. *J. Phys. Chem. C* **2015**, *119*, 26611-26619; (e) Goldsmith, B. R.; Hwang, T.; Seritan, S.; Peters, B.; Scott, S. L. *J. Am. Chem. Soc.* **2015**, *137*, 9604-9616; (f) Fleischman, S. D.; Scott, S. L. *J. Am. Chem. Soc.* **2011**, *133*, 4847-4855; (g) Hisamoto, M.; Nelson, R. C.; Lee, M.-Y.; Eckert, J.; Scott, S. L. *J. Phys. Chem. C* **2009**, *113*, 8794-8805; (h) Moses, A. W.; Raab, C.; Nelson, R. C.; Leifeste, H. D.; Ramsahye, N. A.; Chattopadhyay, S.; Eckert, J.; Chmelka, B. F.; Scott, S. L. *J. Am. Chem. Soc.* **2007**, *129*, 8912-8920; (i) Moses, A. W.; Ramsahye, N. A.; Raab, C.; Leifeste, H. D.; Chattopadhyay, S.; Chmelka, B. F.; Eckert, J.; Scott, S. L. *Organometallics* **2006**, *25*, 2157-2165; (j) Richmond, M. K.; Scott, S. L.; Yap, G. P. A.; Alper, H. *Organometallics* **2002**, *21*, 3395-3400; (k) Beaudoin, M. C.; Womiloju, O.; Fu, A.; Ajjou, J. A. N.; Rice, G. L.; Scott, S. L. *J. Mol. Catal. A: Chem.* **2002**, *190*, 159-169; (l) Richmond, M. K.; Scott, S. L.; Alper, H. *J. Am. Chem. Soc.* **2001**, *123*, 10521-10525; (m) Bouh, A. O.; Rice, G. L.; Scott, S. L. *J. Am. Chem. Soc.* **1999**, *121*, 7201-7210; (n) Ajjou, J. A. N.; Scott, S. L.; Paquet, V. *J. Am. Chem. Soc.* **1998**, *120*, 415-416; (o) Ajjou, J. A. N.; Scott, S. L. *Organometallics* **1997**, *16*, 86-92.

16. (a) Boukebbous, K.; Merle, N.; Larabi, C.; Garron, A.; Darwich, W.; Laifa, E. A.; Szeto, K.; De Mallmann, A.; Taoufik, M. *New J. Chem.* **2017**, *41*, 427-431; (b) Fedorov, A.; Liu, H.-J.; Lo, H.-K.; Copéret, C. *J. Am. Chem. Soc* **2016**, *138*, 16502-16507; (c) Uberman, P. M.; Costa, N. J. S.; Philippot, K.; C. Carmona, R.; Dos Santos, A. A.; Rossi, L. M. *Green Chem.* **2014**, *16*, 4566-4574; (d) Serna, P.; Gates, B. C. *Acc. Chem. Res.* **2014**, *47*, 2612-2620; (e) Merlo, A. B.; Vetere, V.; Casella, M. L. *Curr. Catal.* **2014**, *3*, 244-253; (f) Thomas, J. M.; Raja, R. *J. Organomet. Chem.* **2004**, *689*, 4110-4124; (g) Didillon, B.; Le Peltier, F.; Candy, J. P.; Boitiaux, J. P.; Basset, J. M. *Stud. Surf. Sci. Catal.* **1992**, *73*, 23-30.

17. (a) Santori, G. F.; Casella, M. L.; Ferretti, O. A. *J. Mol. Catal. A Chem.* **2002**, *186*, 223-239; (b) Hermans, S.; Raja, R.; Thomas, J. M.; Johnson, B. F.; Sankar, G.; Gleeson, D. *Angew. Chem., Int. Ed.* **2001**, *40*, 1211-1215; (c) Santori, G. F.; Casella, M. L.; Siri, G. J.; Adúriz, H. R.; Ferretti, O. A. *Appl. Catal. A* **2000**, *197*, 141-149; (d) Gallezot, á.; Richard, D. *Catal. Rev.* **1998**, *40*, 81-126; (e) Claus, P. *Top. Catal.* **1998**, *5*, 51-62; (f) Candy, J.-P.; Didillon, B.; Smith, E. L.; Shay, T. B.; Basset, J.-M. *J. Mol. Catal.* **1994**, *86*, 179-204; (g) Didillon, B.; Candy, J.; El Mansour, A.; Houtmann, C.; Basset, J.-M. *J. Mol. Catal.* **1992**, *74*, 43-49; (h) Lecuyer, C.; Quignard, F.; Choplin, A.; Olivier, D.; Basset, J. M. *Angew. Chem., Int. Ed.* **1991**, *30*, 1660-1661; (i) Ferretti, O.; Bournonville, J.; Mabilon, G.; Martino, G.; Candy, J.; Basset, J.-M. *J. Mol. Catal.* **1991**, *67*, 283-294; (j) Agnelli, M.; Louessard, P.; El Mansour, A.; Candy, J.; Bournonville, J.; Basset, J. *Catal. Today* **1989**, *6*, 63-72; (k) Ugo, R. *Cat. Rev. - Sci. Eng.* **1975**, *11*, 225-297.

18. (a) Cybulskis, V. J.; Bukowski, B. C.; Tseng, H.-T.; Gallagher, J. R.; Wu, Z.; Wegener, E.; Kropf, A. J.; Ravel, B.; Ribeiro, F. H.; Greeley, J.; Miller, J. T. *ACS Catal.* **2017**, *7*, 4173-4181; (b) Qi, Z.; Xiao, C.; Liu, C.; Goh, T. W.; Zhou, L.; Maligal-Ganesh, R.; Pei, Y.; Li, X.; Curtiss, L. A.; Huang, W. *J. Am. Chem. Soc.* **2017**, *139*, 4762-4768; (c) Iihama, S.; Furukawa, S.; Komatsu, T. *ACS Catal.* **2016**, *6*, 742-746; (d) Zhu, J.; Zheng, X.; Wang, J.; Wu, Z.; Han, L.; Lin, R.; Xin, H. L.; Wang, D. *J. Mater. Chem. A Energy Sustain.* **2015**, *3*, 22129-22135; (e) Sode, A.; Musgrove, A.; Bizzotto, D. *J. Phys. Chem. C* **2010**, *114*, 546-553; (f) Miura, A.; Wang, H.; Leonard, B. M.; Abruna, H. D.; Di Salvo, F. J. *Chem. Mater.* **2009**, *21*, 2661-2667.

19. Camacho-Bunquin, J.; Shou, H.; Aich, P.; Beaulieu, D. R.; Klotzsch, H.; Bachman, S.; Marshall, C. L.; Hock, A.; Stair, P. *Rev. Sci. Instrum.* **2015**, *86*, 084103.

20. Camacho-Bunquin, J.; Aich, P.; Ferrandon, M.; Das, U.; Dogan, F.; Curtiss, L. A.; Miller, J. T.; Marshall, C. L.; Hock, A. S.; Stair, P. C. *J. Catal.* **2017**, *345*, 170-182.

21. (a) Becke, A. D. *J. Phys. Chem.* **1993**, *98*, 5648-5652; (b) Lee, C.; Yang, W.; Parr, R. G. *Phys. Rev. B* **1988**, *37*, 785-789.

22. Schafer, A.; Huber, C.; Ahlrichs, R. *J. Phys. Chem.* **1994**, *100*, 5829-5835.

23. Gaussian 09, R. E., Frisch, M. J.; Trucks, G. W.; Schlegel, H. B.; Scuseria, G. E.; Robb, M. A.; Cheeseman, J. R.; Scalmani, G.; Barone, V.; Mennucci, B.; Petersson, G. A.; Nakatsuji, H.; Caricato, M.; Li, X.; Hratchian, H. P.; Izmaylov, A. F.; Bloino, J.; Zheng, G.; Sonnenberg, J. L.; Hada, M.; Ehara, M.; Toyota, K.; Fukuda, R.; Hasegawa, J.; Ishida, M.; Nakajima, T.; Honda, Y.; Kitao, O.; Nakai, H.; Vreven, T.; Montgomery, J. A., Jr.; Peralta, J. E.; Ogliaro, F.; Bearpark, M.; Heyd, J. J.; Brothers, E.; Kudin, K. N.; Staroverov, V. N.; Kobayashi, R.; Normand, J.; Raghavachari, K.; Rendell, A.; Burant, J. C.; Iyengar, S. S.; Tomasi, J.; Cossi, M.; Rega, N.; Millam, J. M.; Klene, M.; Knox, J. E.; Cross, J. B.; Bakken, V.; Adamo, C.; Jaramillo, J.; Gomperts, R.; Stratmann, R. E.; Yazyev, O.; Austin, A. J.; Cammi, R.; Pomelli, C.; Ochterski, J. W.; Martin, R. L.; Morokuma, K.; Zakrzewski, V. G.; Voth, G. A.; Salvador, P.; Dannenberg, J. J.; Dapprich, S.; Daniels, A. D.; Farkas, Ö.; Foresman, J. B.; Ortiz, J. V.; Cioslowski, J.; Fox, D. J. Gaussian, Inc., Wallingford CT, 2009.

24. Das, U.; Zhang, G.; Hu, B.; Hock, A. S.; Redfern, P. C.; Miller, J. T.; Curtiss, L. A. *ACS Catal.* **2015**, *5*, 7177-7185.

25. Zagdoun, A.; Casano, G.; Ouari, O.; Schwarzwälder, M.; Rossini, A. J.; Aussenac, F.; Yulikov, M.; Jeschke, G.; Copéret, C.; Lesage, A.; Tordo, P.; Emsley, L. *J. Am. Chem. Soc* **2013**, *135*, 12790-12797.

26. (a) Gansmüller, A.; Simorre, J.-P.; Hediger, S. *J. Magn. Reson.* **2013**, *234*, 154-164; (b) Dvinskikh, S. V.; Zimmermann, H.; Maliniak, A.; Sandström, D. *J. Magn. Reson.* **2004**, *168*, 194-201.

27. Larsen, F. H.; Jakobsen, H. J.; Ellis, P. D.; Nielsen, N. C. *J. Magn. Reson.* **1998**, *131*, 144-147.

28. Perras, F. A.; Wang, Z.; Naik, P.; Slowing, I. I.; Pruski, M. *Angew. Chem., Int. Ed.* **2017**, *56*, 9165-9169.

29.Perras, F. A.; Kobayashi, T.; Pruski, M. *J. Am. Chem. Soc.* **2015**, *137*, 8336-8339.

30. Bielecki, A.; Kolbert, A. C.; Levitt, M. H. *Chem. Phys. Lett.* **1989**, *155*, 341-346.

31. Harris, K. J.; Lupulescu, A.; Lucier, B. E. G.; Frydman, L.; Schurko, R. W. *J. Magn. Reson.* **2012**, *224*, 38-47.

32. Kupce, E.; Freeman, R. *J. Magn. Reson.* **1995**, *115*, 273-276.

33. O'Dell, L. A.; Schurko, R. W. *Chem. Phys. Lett.* **2008**, *464*, 97-102.

34. Schweitzer, N. M.; Hu, B.; Das, U.; Kim, H.; Greeley, J.; Curtiss, L. A.; Stair, P. C.; Miller, J. T.; Hock, A. S. *ACS Catal.* **2014**, *4*, 1091-1098.

35. (a) Kobayashi, T.; Perras, F. A.; Slowing, I. I.; Sadow, A. D.; Pruski, M. *ACS Catal.* **2015**, *5*, 7055; (b) Rossini, A. J.; Zagdoun, A.; Lelli, M.; Lesage, A.; Copéret, C.; Emsley, L. *Acc. Chem. Res.*

2013, *46*, 1942-1951; (c) Lesage, A.; Lelli, M.; Gajan, D.; Caporini, M. A.; Vitzthum, V.; Miéville, P.; Alauzun, J.; Roussey, A.; Thieuleux, C.; Mehdi, A. *J. Am. Chem. Soc* **2010**, *132*, 15459-15461; (d) Maly, T.; Debelouchina, G. T.; Bajaj, V. S.; Hu, K.-N.; Joo, C.-G.; Mak–Jurkauskas, M. L.; Sirigiri, J. R.; van der Wel, P. C.; Herzfeld, J.; Temkin, R. J. *J. Phys. Chem.* **2008**, *128*, 02B611.
36. Xue, Z.; Strouse, M. J.; Shuh, D. K.; Knobler, C. B.; Kaesz, H. D.; Hicks, R. F.; Williams, R. S. *J. Am. Chem. So* **1989**, *111*, 8779-8784.
37. Kobayashi, T.; Perras, F. A.; Chaudhary, U.; Slowing, I. I.; Huang, W.; Sadow, A. D.; Pruski, M. *Solid State Nucl. Magn. Reson.* **2017**, *87*, 38-44.
38. Kobayashi, T.; Perras, F. A.; Goh, T. W.; Metz, T. L.; Huang, W.; Pruski, M. *J. Phys. Chem. Lett.* **2016**, *7*, 2322-2327.
39. Still, B. M.; Kumar, P. G. A.; Aldrich-Wright, J. R.; Price, W. S. *Chem. Soc. Rev.* **2007**, *36*, 665-686.
40. Pregosin, P. S., Platinum NMR Spectroscopy. In *Annual Reports on NMR Spectroscopy*, Webb, G. A., Ed. Academic Press: **1986**, *17*, 285-349.
41. Boardman, L. D.; Newmark, R. A. *Magn. Reson. Chem.* **1992**, *30*, 481-489.
42. Zagdoun, A.; Casano, G.; Ouari, O.; Schwarzwälder, M.; Rossini, A. J.; Aussenac, F.; Yulikov, M.; Jeschke, G.; Copéret, C.; Lesage, A. *J. Am. Chem. Soc* **2013**, *135*, 12790-12797.
43. (a) Zhang, N.; Han, C.; Xu, Y.-J.; Foley Iv, J. J.; Zhang, D.; Codrington, J.; Gray, S. K.; Sun, Y. *Nat. Photonics* **2016**, *10*, 473; (b) Czaplinska, J.; Decyk, P.; Ziolek, M. *Appl. Catal. A: Gen.* **2015**, *504*, 361-372; (c) Sortino, S.; Petralia, S.; Conoci, S.; Di Bella, S. *J. Mater. Chem.* **2004**, *14*, 811-813.
44. (a) Andrews, L.; Wang, X.; Manceron, L. *J. Phys. Chem.* **2001**, *114*, 1559-1566; (b) Prokopchuk, E. M.; Jenkins, H. A.; Puddephatt, R. J. *Organometallics* **1999**, *18*, 2861-2866; (c) Yoshida, T.; Yamagata, T.; Tulip, T.; Ibers, J. A.; Otsuka, S. *J. Am. Chem. Soc* **1978**, *100*, 2063-2073; (d) Gavrllova, I.; Gelhman, M. *Russ. J. Inorg. Chem.* **1971**, *16*, 596; (e) Clark, H.; Tsang, W. *J. Am. Chem. Soc* **1967**, *89*, 529-533.
45. Martin, D.; Duprez, D. *J. Phys. Chem. B* **1997**, *101*, 4428-4436.
46. (a) Liu, S.; Tan, J. M.; Gulec, A.; Crosby, L. A.; Drake, T. L.; Schweitzer, N. M.; Delferro, M.; Marks, L. D.; Marks, T. J.; Stair, P. C. *Organometallics* **2017**, *36*, 818-828; (b) Ding, K.; Gulec, A.; Johnson, A. M.; Schweitzer, N. M.; Stucky, G. D.; Marks, L. D.; Stair, P. C. *Science* **2015**, *350*, 189-192; (c) Kistler, J. D.; Chotigkrai, N.; Xu, P.; Enderle, B.; Praserthdam, P.; Chen, C.-Y.; Browning, N. D.; Gates, B. C. *Angew. Chem., Int Ed.* **2014**, *53*, 8904-8907; (d) Moses-DeBusk, M.; Yoon, M.; Allard, L. F.; Mullins, D. R.; Wu, Z.; Yang, X.; Veith, G.; Stocks, G. M.; Narula, C. K. *J. Am. Chem. Soc* **2013**, *135*, 12634-12645; (e) Akdogan, Y.; Vogt, C.; Bauer, M.; Bertagnolli, H.; Giurgiu, L.; Roduner, E. *Phys. Chem. Chem. Phys.* **2008**, *10*, 2952-2963; (f) Panagiotopoulou, P.; Christodoulakis, A.; Kondarides, D. I.; Boghosian, S. *J. Catal.* **2006**, *240*, 114-125.
47. Qiao, B.; Wang, A.; Yang, X.; Allard, L. F.; Jiang, Z.; Cui, Y.; Liu, J.; Li, J.; Zhang, T. *Nat. Chem.* **2011**, *3*, 634-641.
48. Forniés, J.; Gómez-Saso, M. A.; Martín, A.; Martínez, F.; Menjón, B.; Navarrete, J. *Organometallics* **1997**, *16*, 6024-6027.
49. Liu, J. *ACS Catal.* **2017**, *7*, 34-59.
50. Pt is generally not very active for aldehyde and ketone hydrogenation.

Table of Content Graphic